Review of Scientific Instruments

Thermocouple-tip-exposing temperature assessment technique for evaluating photothermal conversion efficiency of plasmonic nanoparticles at low laser power density

Cite as: Rev. Sci. Instrum. **90**, 094902 (2019); https://doi.org/10.1063/1.5109117
Submitted: 06 May 2019 . Accepted: 31 August 2019 . Published Online: 20 September 2019

Muzhaozi Yuan, Ya Wang, David Hwang, and Jon P. Longtin

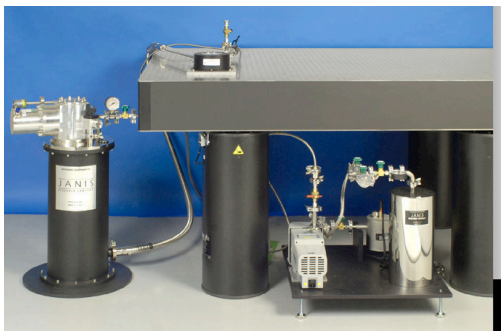

AIP Publishing

Review of Scientific Instruments ARTICLE scitation.org/journal/rsi

Thermocouple-tip-exposing temperature assessment technique for evaluating photothermal conversion efficiency of plasmonic nanoparticles at low laser power density

Cite as: Rev. Sci. Instrum. 90, 094902 (2019); doi: 10.1063/1.5109117
Submitted: 6 May 2019 • Accepted: 31 August 2019 •
Published Online: 20 September 2019

Muzhaozi Yuan,[1] Ya Wang,[1,a)] David Hwang,[2] and Jon P. Longtin[2]

AFFILIATIONS

[1]J. Mike Walker '66 Department of Mechanical Engineering, Texas A and M University, College Station, Texas 77840-3123, USA
[2]Department of Mechanical Engineering, Stony Brook University, Stony Brook, New York 11794-2300, USA

[a)]**Author to whom correspondence should be addressed:** ya.wang@tamu.edu

ABSTRACT

A new thermocouple (TC) tip-exposing temperature assessment technique that combines experimental temperature measurements with a numerical model of the photothermal conversion efficiency η is presented. The proposed technique is designed to evaluate η for a gold-coated superparamagnetic iron oxide nanoparticle (SPIO-Au NP) solution (26 nm, 12–70 ppm) at low continuous wave laser power (103 mW, 532 nm) irradiation in a convenient manner under ambient conditions. The TC tip temperature is measured during the first 30 s of the laser exposure, and the results are combined with a finite element model to simulate the temperature rise of the NP solution for a given concentration. The value of η is adjusted in the model until the model agrees with the measured transient TC temperature rise. Values of $\eta = 1.00$ were observed for all concentrations. Theoretical predictions of η derived by Mie theory confirmed the near unity conversion efficiency of the as-synthesized SPIO-Au NPs. Advantages of the current technique include co-locating the TC tip in the geometric center of the laser-heated region, rather than outside of this region. In addition, the technique can be done under ambient room conditions using unmodified commercially available hardware.

I. INTRODUCTION

Photothermal therapy is based on the principle that the plasmonic nanoparticles (NPs) delivered into targeted areas can be irradiated by a laser, which causes the synchronized oscillations of conduction free electrons at the laser wavelength, and leads to the absorption and/or scattering of an incident photon.[1] Only photons that are absorbed are converted into thermal energy. The *photothermal conversation efficiency*, η, is defined as the number of photons absorbed divided by the combined number of photons absorbed and scattered. Among various plasmonic NPs, gold-based NPs are promising for therapeutic photothermal therapy platforms because of their superior optical properties,[2–8] excellent stability, and biocompatibility.[9,10] Au NPs are also straightforward to surface-functionalize[11–14] with targeted ligands or therapeutic agents via well-developed Au-thiol chemistry.[15,16] An effective strategy of theranostic NPs for photothermal therapy of cancer cell treatment is to imbed multiple diagnostic and therapeutic functions on one single nanoparticle to construct a theranostic nanoplatform.[17] Superparamagnetic iron oxide (SPIO) NPs are widely used for medical imaging as the contrast agent.[16] Moreover, magnetic NPs can be used for magnetic targeting with an external magnetic field, which can enhance the cell uptake of NPs and improve the agent accumulation located in the tumor area.[18] Therefore, SPIO-Au core-shell NPs, combining the benefit of magnetic NPs and plasmonic properties of Au, are an attractive and promising nanomedicine for the photothermal therapy of cancer treatment.[5,7]

In order to use SPIO-Au NPs for photothermal therapy, it is necessary to measure the photothermal properties of SPIO-Au NPs.

One technique was developed in 2007 by Roper *et al.*,[3] in which a custom cuvette was filled, sealed with epoxy, and placed in a vacuum environment to measure the temperature profile of Au NPs [20 nm diameter, 920 ppm in deionized (DI) water, 7.9 μl, 350 s to reach equilibrium] using a 514 nm continuous wave (CW) laser (0.17 W, 3 mm beam size). According to their modeling and calculation of the cuvette heating temperature vs time, they estimated the photothermal conversion efficiency η of Au NPs at 920 ppm to be 0.034, which was notably lower than expected from theoretical estimates. Possible reasons for this discrepancy include convection and radiation cooling effects that were not included and inaccuracies in the liquid temperature measurement since the thermocouple (TC) sensor was not in direct contact with the laser-irradiated region of the NP solution but rather connected to the exterior of the test cell.

Roper's method has been used by other researchers as well to measure the photothermal conversion efficiency of other recently synthesized plasmonic NPs.[18–20] Following the same method, Feng *et al.*[19] measured the photothermal conversion efficiency ($\eta = 0.24$) of Au/Polypyrrole@Fe_3O_4 NPs (200 nm, 1400 ppm) using an 808 nm laser at a power density of 2 W/cm^2. Hu *et al.*[18] tested the photothermal conversion efficiency ($\eta = 0.1$) of Au-coated Fe_3O_4 NPs (100 nm, 0.78–100 ppm) using an 808 nm laser irradiation at 15 W/cm^2. Wang *et al.*[20] measured the photothermal conversion efficiency ($\eta = 0.618$) of $MoSe_2$ nanoflowers (150–180 nm, 75 ppm) using an 808 nm laser at a power density of 1 W/cm^2.

As an alternative to the time constant method developed by Roper *et al.*,[3] Jiang *et al.*[4] used a mechanical stirrer to reduce the temperature gradients in the Au NPs solution (5–50 nm, 39.4 ppm, 1 ml) inside a standard cuvette during the laser irradiation (532 nm, 0.228 W, 2 mm beam size). It took at least 1200 s to reach an equilibrium temperature. The photothermal conversion efficiency was size-dependent but reached 0.737 for Au NPs of 18 nm in diameter, which is significantly larger than the ~0.03 value measured by Roper *et al.* for otherwise very similar particles.

Richardson *et al.*[2] developed an alternative experimental technique in which a 10 μl drop of Au NPs solution (20 nm, 45 ppm) was suspended from a syringe needle with thermocouple (TC) tip inside the droplet to measure the temperature profile of NPs under a 532 nm CW laser (0.14 W, 0.23 W, and 0.28 W). The time to reach steady-state was about 50 s. Using their measurement setup, values of η very close to unity (0.97–1.03) were observed, which was in agreement with expected values of η near-unity because of the nearly zero quantum yield (10^{-6}).[21] However, this technique requires careful control of the syringe droplet, and evaporation of the NPs solution during the laser irradiation complicates the thermal analysis.

This work addresses the concerns above by developing a new photothermal conversion efficiency that provides accuracy and ease of use. Unlike previous methods, the TC tip in this technique is placed in the center of the heating laser beam to ensure that the temperature measured is that of the NP solution itself. A standard plastic cuvette is used to contain the NP solution. The self-heating of the thermocouple by the laser is incorporated, and a three-dimensional finite element model (FEM) using COMSOL Multiphysics® was developed to capture the heat transfer in the system during the initial 30 s of laser exposure. By restricting the measurement duration to ~30 s, the characteristic heat diffusion length is smaller than the cuvette dimensions so that natural convection and the influence of the container geometry on the heat transfer can be neglected.[22] The proposed technique is used to measure the temperature profile of lab-synthesized SPIO-Au NPs under the 532 nm CW laser illumination.

II. THEORETICAL BASIS AND METHODS

A. TC-tip-exposing temperature assessment technique

Referring to Fig. 1 to measure the temperature profile of the NP solution, a polystyrene (PS) semimicro cuvette (12.5 × 12.5 × 45 mm^3 outer dimensions) is filled with 0.5 ml of NP solution. An MGL-FN-532 (CNI Optoelectronics) CW laser provides a Gaussian beam profile with beam radius $r_0 = 1.5$ mm (where the intensity values fall to $1/e^2$ of the axial intensity value, and e is the base of natural logarithm) and a power of 103 mW that is directed horizontally through the middle of the liquid in the cuvette (cuvette inner depth: $d = 10$ mm). A K-type TC-tip (Omega Engineering) with 0.040 mm lead wires and a bead diameter of 0.080 mm is placed in the geometric center ($x = 0, z = 0$) of the laser-illuminated liquid region. The TC tip is located approximately $y = 3$ mm from the inner cuvette wall facing the incident laser beam to ensure that the temperature sensor and the heating laser are located in the same region of the liquid. Due to the extremely small size of NPs (26 nm) compared with the TC tip size, the effect of NPs dispersity on temperature measurement

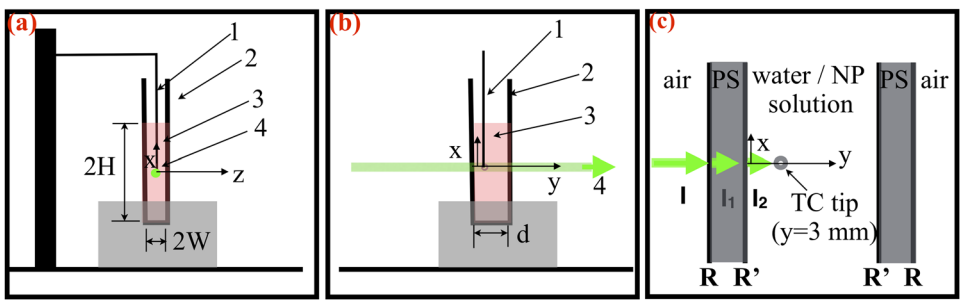

FIG. 1. Experimental setup of the temperature profile measurement of SPIO-Au NP solutions. (a) Experimental setup (front view), (b) experimental setup (side view), and (c) detail of laser path through the cuvette containing DI water/NPs solution. Here, (1) thermocouple (Omega, Stamford, CT, K-type, 0.040 mm wire, 0.080 mm bead diameter); (2) BRAND polystyrene (PS) cuvette, (3) SPIO-Au NPs solution, and (4) MGL-FN-532 (nm)-103 mW (PSU-H-FDA) laser.

can be neglected. Also, the NPs solution was sonicated for 5 min at 80 kHz for uniform dispersion of NPs before measurements. The test is performed in ambient conditions (vacuum not required). The temperature profile of the DI water and the NP solution at different concentrations were measured using this proposed TC-tip-exposing method under the excitation of a 532 nm CW laser.

Figure 1(c) shows the 532 nm CW laser path through the cuvette and the liquid. Here, I represented the incident laser intensity. I_1 is the laser intensity inside the front wall of the cuvette, which is made of polystyrene (PS) and is 1 mm thick, and I_2 represents the laser intensity when the laser leaves the front PS wall and enters the liquid. These intensities represent the spatially averaged intensity based on overall laser power and beam radius.

The refractive indices of the air, PS wall, and water are $n_{air} = 1.00$, $n_{PS} = 1.59$, and $n_{water} = 1.33$, respectively. The reflectance between the air and the PS wall can be obtained from

$$R = \left(\frac{n_{air} - n_{ps}}{n_{air} + n_{ps}}\right)^2 = 0.052, \tag{1}$$

while the reflectance between the DI water and the PS is

$$R' = \left(\frac{n_{water} - n_{ps}}{n_{water} + n_{ps}}\right)^2 = 0.008. \tag{2}$$

Then, the intensities in the PS wall and front of the liquid ($y = 0$) are

$$I_1 = (1 - R)I, \tag{3}$$

$$I_2 = (1 - R)(1 - R')I. \tag{4}$$

B. Finite element simulation

1. Laser beam description

The incident laser beam propagates in the z direction. The Gaussian incident laser intensity (W/cm^2) can be expressed as

$$I(r) = I_0 e^{-2\left(\frac{r}{r_0}\right)^2} = \frac{2I_m}{\pi r_0^2} e^{-2\left(\frac{r}{r_0}\right)^2}, \tag{5}$$

where $I_m = 103$ mW is the total incident laser power (mW) measured by a Coherent FieldMate laser power meter and I_0 is the maximum laser intensity at the centerline of the beam. In Cartesian coordinates, the beam intensity becomes

$$I(x, z) = \frac{2I_m}{\pi r_0^2} e^{\frac{-2(x^2+z^2)}{r_0^2}}, \tag{6}$$

where the center of the laser beam is located at $x = 0$, $z = 0$, i.e., the centerline of the liquid region shown in Fig. 1(a) as the laser beam propagates along the y direction.

TABLE I. Thermal properties for analysis.

Material	Density, ρ (kg/m^3)	Thermal conductivity, k (W/m K)	Specific heat, C_p (J/kg K)
NP solution	0.9982	0.6	4180
Chromel	8730	17.3	448
Alumel	8610	29.7	523

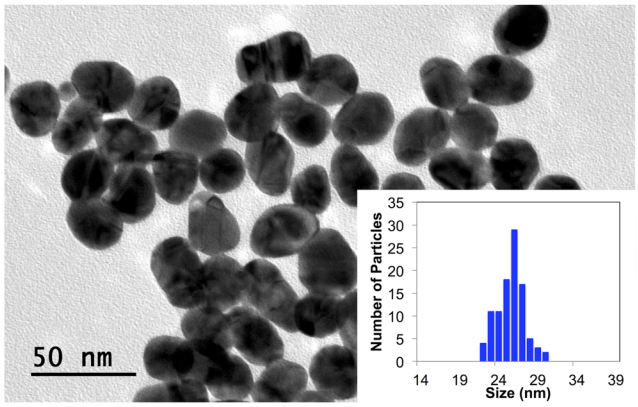

FIG. 2. Morphology and size distribution for Au-coated SPIO NPs of diameter 26 nm (8 nm Au coating). Histogram indicates size distribution for 100 NPs in total. Note that narrow size distribution and uniform quasispherical morphology.

A finite element model (FEM) was developed using COMSOL Multiphysics to simulate the temperature profile of SPIO-Au NPs irradiated under low laser power. The SPIO-Au NPs aqueous solution in the cuvette has dimensions $2W = 4.5$ mm, $2H = 23$ mm, and $d = 10$ mm, as shown in Figs. 1(a) and 1(b). The transient heat conduction equation is used to determine the time-dependent temperature history of the NP solution and the thermocouple

$$\rho_i C_{p,i} \frac{\partial T_i}{\partial t} = k_i \left(\frac{\partial^2 T_i}{\partial x^2} + \frac{\partial^2 T_i}{\partial y^2} + \frac{\partial^2 T_i}{\partial z^2}\right) + \dot{Q}_i(x, y, z), \tag{7}$$

where ρ is the density, C_p is the specific heat, k is the thermal conductivity, $i = np$ for the NP solution, and $i = tc$ for the thermocouple. The temperature $T = T(x, y, z, t)$ varies with both the position and time.

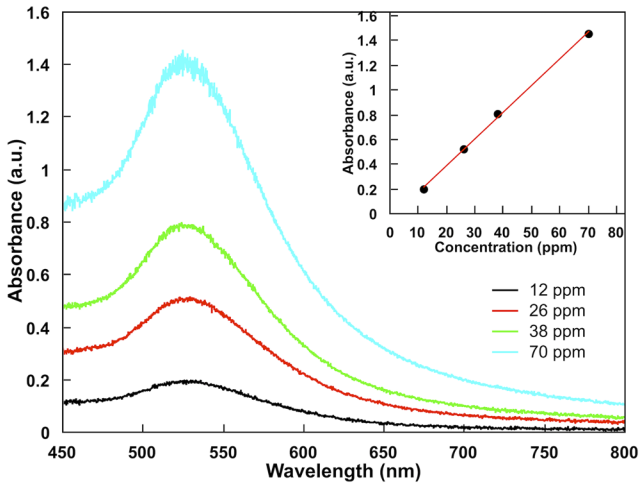

FIG. 3. Light absorption spectra of the 26 nm SPIO-Au NP solutions indicating the peak absorbance value increased at higher concentrations (12, 26, 38, 70 ppm) and the insert indicating the linear relationship between the peak absorbance and the concentration.

TABLE II. α and A values for different concentrations of SPIO-Au NPs.

Concentration (ppm)	12	26	38	70
Absorbance, A	0.199	0.505	0.781	1.416
Absorption coefficient, α (1/m)	45.8	116.3	179.8	326.0

In the numerical solution, the TC alloys are further distinguished between the chromel leg, the alumel leg, and the bead since each has different ρ, C_p, and k. The TC bead is modeled as a sphere of diameter 0.080 mm, with thermophysical properties k, ρ, and C_p taken as the average of the corresponding properties for the chromel and alumel. The chromel leg extends vertically upward ($x > 0$, $z = 0$), and the alumel leg extends vertically downward ($x < 0$, $z = 0$).

The boundary conditions are as follows. For the NP solution,

$$T_{np}(x, y, z, t) = T_\infty, \quad \text{at} \quad x = \pm W, \tag{8a}$$

$$T_{np}(x, y, z, t) = T_\infty, \quad \text{at} \quad z = \pm H, \tag{8b}$$

$$T_{np}(x, y, z, t) = T_\infty, \quad \text{at} \quad y = 0 \quad \text{and} \quad y = d, \tag{8c}$$

where T_∞ is the ambient temperature.

For the TC, the boundary conditions are that the temperature and heat flux are continuous at the TC surface

$$T_{tc} = T_{np}, \tag{9a}$$

$$k_{tc}\frac{\partial T_{tc}}{\partial n} = k_{np}\frac{\partial T_{np}}{\partial n}, \tag{9b}$$

where n is the direction normal to the TC at the point of interest.

The initial condition for the entire system is

$$T_i(x, y, z, t) = T_\infty, \quad \text{at} \quad t = 0. \tag{10}$$

The thermodynamic properties for the NP solution and the thermocouple alloys chromel and alumel are shown in Table I. Because the NP concentration is low, the NP solution properties for DI water are used.

2. Heat-source terms

The volumetric heating source (W/m^3) in Eq. (7) for the TC as a result of direct heating by the incident laser light is

$$\dot{Q}_{tc}(x, z) = \beta I_2 e^{-\alpha\delta} e^{-2(x^2+z^2)/r_0^2}, \tag{11}$$

where $\delta = 3$ mm is the TC tip distance from the front cuvette wall through which the incident laser light enters to the TC tip location

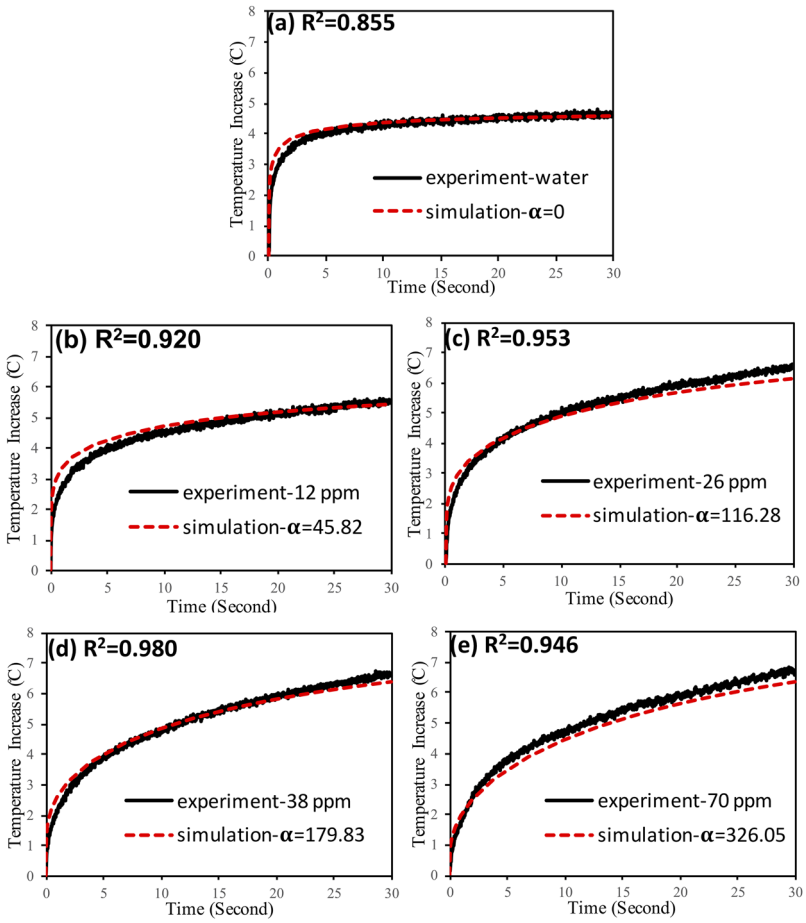

FIG. 4. Comparison of measured temperature increases from experiments vs simulated temperature increases from the FEM modeling during the very first 30 s for (a) water (α = 0); (b) NPs solution at 12 ppm (α = 45.8 1/m); (c) NPs solution at 26 ppm (α = 116.3 1/m); (d) NPs solution at 38 ppm (α = 179.8 1/m); and (e) NPs solution at 70 ppm (α = 326.0 1/m). The value of R^2 represents how close the simulation results are to the experimental data, with higher values better.

in the NP solution and α is the absorption coefficient obtained from the measured absorbance A: $\alpha = -\ln(10^{-A})/d$. The absorbance A was measured using a Flame miniature spectrometer (FLAME-S-XR1-ES, Ocean Optics, Inc.) at a wavelength of 532 nm and an optical path length $d = 10$ mm.

The heating coefficient for the TC is determined by replacing the NP solution with DI water and measuring the transient laser heating. The DI water does not absorb the laser light; hence, the only source of heating is the TC itself. The TC heating coefficient, β, in Eq. (11) is then adjusted in the numerical model until the model and data agree.

The laser intensity in the NPs solution, after accounting for reflections in the front cuvette wall, is

$$I(x,y,z) = I_2 e^{-\alpha y} e^{-2(x^2+z^2)/r_0^2}. \quad (12)$$

The laser light is attenuated as it passes through the NP solution due to absorption and scattering, i.e., $\frac{dI}{dy} < 0$. The fraction of light absorbed, η, is the photothermal conversion efficiency and contributes to the NP solution heating

$$\dot{Q}_{np}(x,y,z) = -\eta \frac{dI}{dy} = \eta \alpha I_2 e^{-\alpha y} e^{-2(x^2+z^2)/r_0^2}. \quad (13)$$

III. RESULTS AND DISCUSSION

Our SPIO-Au NPs were synthesized using the synergistic seed growth and citrate reducing method reported in previous work.[23,24] By the nature of the synthesizing process, the surfaces of SPIO-Au NPs were capped by citrate acid ligands with negative charges, which protected the NPs from agglomeration by the strong repulsive force.[23] Figure 2 shows a transmission electron microscope image of the SPIO-Au NPs. The particles have a quasispherical shape and narrow size distribution that averages 26 nm.

Figure 3 shows the absorbance vs wavelength of the SPIO-Au NP solutions (26 nm) at different concentrations (12, 26, 38, 70 ppm). The inset in the figure indicates the linear relationship between absorbance and the concentration, which agrees well with Beer's law of absorption. The absorbance A and the corresponding absorption coefficient α of the NPs solutions at different concentrations at the laser wavelength of 532 nm are listed in Table II. ($\alpha = A = 0$ for DI water.)

By comparing this FEM simulation with the temperature profile measurement, the photothermal conversion efficiency η of unknown plasmonic NPs can be determined using the following procedure: first, the temperature profile with the TC in DI water is measured to determine β, followed by a measurement with the NPs of interest. The temperature history during the first 30 s of the laser heating is recorded. The thermal model [Eq. (7)] and the heat source equations [Eqs. (11) and (13) with unknown η] are used to simulate the transient temperature history of the thermocouple in the NP solution. The value of η in Eq. (13) is adjusted until the simulation matches the measured temperature profile as closely as possible.

The measured and calculated temperature profiles for pure DI water and NPs at concentrations of 12, 26, 38, and 70 ppm are shown in Fig. 4. Figure 4(a) is for the DI water only. For this case, the heat source is from the TC tip only; thus, $\dot{Q}_{np} = 0$. The best agreement

TABLE III. The photothermal efficiency for different concentrations of SPIO-Au NPs.

Concentration (ppm)	12	26	38	70
Photothermal conversion efficiency η	1.00	1.00	1.00	1.00
Coefficient of determination R^2	0.920	0.953	0.980	0.946

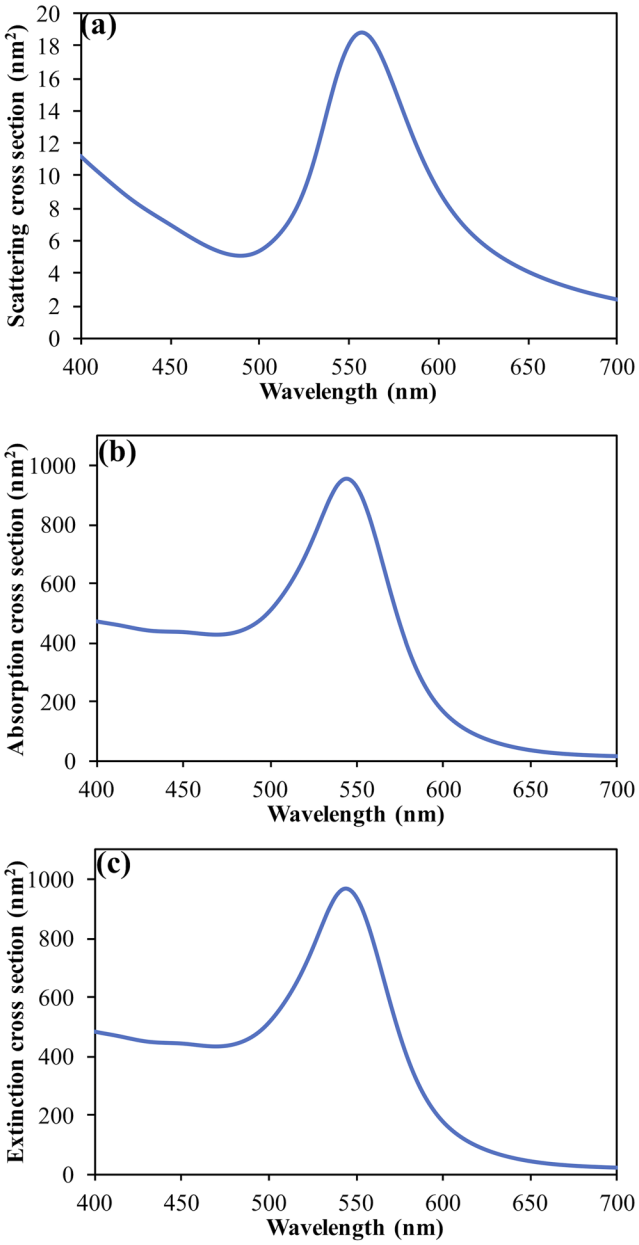

FIG. 5. (a) Scattering cross section (10.87 nm^2 at 532 nm), (b) absorption cross section (831.53 nm^2 at 532 nm), and (c) extinction cross section (842.40 nm^2 at 532 nm) for 26 nm SPIO-Au NPs (SPIO core diameter: 10 nm, Au shell thickness: 6.5 nm) calculated based on the MNPBEM toolbox.

with the simulated temperature profile for DI water was found to be $\beta = 118\,600\ m^{-1}$.

Next, the simulation of the temperature profile with the NPs solution was performed. For each NP concentration, the numerical model was evaluated with values of η ranging from 0 to 1. The goodness-of-fit parameter, R^2, was calculated, and η was adjusted to maximize R^2. The results are shown in Fig. 4. It can be seen that the simulated temperature history agrees very well with the experimental measurement within the first 30 s. Table III lists the best-fit value of the photothermal conversion efficiency for each concentration and the corresponding value of R^2. It was found that in all cases, a photothermal conversion efficiency of unity ($\eta = 1.00$) yielded the best fit. This finding is in consistent with the literature[2] that ultrasmall plasmonic NPs (~20 nm) have extremely low optical quantum yields (10^{-6}) and almost 100% of the photon energy is converted to heat.

The scattering, absorption, and extinction cross sections of SPIO-Au core shell NPs with 26 nm diameter were studied by using a boundary element method proposed by Hohenester (MNPBEM toolbox).[25] The results are plotted in Fig. 5, and the ratio of absorbance/extinction at the wavelength of 532 nm was calculated to be 0.987 (the absorbance cross section/the extinction cross section at 532 nm). This value is in good agreement with $\eta \cong 1.00$ from the experimental measurements above.

Compared with the traditional temperature profile assessment methods reported in the literature,[2–4] the technique above provides several benefits. First, placing the TC tip in the center of the laser beam assures that the temperature sensor and the heating laser represent the same region in the liquid where the heating due to photothermal conversion occurs. Second, our method involves a fast and simple sample preparation using commercial hardware and can be done in ambient conditions in the laboratory. Third, by combining the experimental measurements with a high-fidelity FEM simulation, we only require the data of the temperature rise for the first 30 s, avoiding the long-time laser heating times required for other techniques, which can introduce additional measurement error due to conduction through the cuvette boundaries, natural convection, and evaporation of the NP solution. The method herein is thermally based; hence, it should be applicable to a wide range of other plasmonic NPs.

IV. CONCLUSIONS

We have developed a novel direct-exposure technique for the measurement of nanoparticle solution photothermal coefficients. A thermocouple is immersed in the nanoparticle solution irradiated directly by a 3 mm diameter, 532 nm CW laser. The heat transfer equations for both the thermocouple and the surrounding nanoparticle solution are formulated and solved for using COMSOL Multiphysics to simulate the temperature profile within the first 30 s of the laser exposure. Using the photothermal conversion coefficient as an adjustable parameter, very good agreement between the model and measurement are found. SPIO-Au NPs with uniform quasispherical shape and narrow size distribution were used in the development of the technique, and the photothermal conversion affinity was found to be near unity as expected from both predictions and other investigations.

ACKNOWLEDGMENTS

This work was supported by Grant Nos. DOE-AR0000531 and DOE-AR0000945. The authors would like to thank the Thermomechanical and Imaging Nanoscale Characterization (ThINC) at Stony Brook University for their assistance of transmission electron microscopy of nanoparticles.

REFERENCES

[1] R. S. Riley and E. S. Day, Wiley Interdiscip. Rev.: Nanomed. Nanobiotechnol. **9**, e1449 (2017).
[2] H. H. Richardson, M. T. Carlson, P. J. Tandler, P. Hernandez, and A. O. Govorov, Nano Lett. **9**, 1139–1146 (2009).
[3] D. K. Roper, W. Ahn, and M. Hoepfner, J. Phys. Chem. C **111**, 3636–3641 (2007).
[4] K. Jiang, D. A. Smith, and A. Pinchuk, J. Phys. Chem. C **117**, 27073–27080 (2013).
[5] J. F. Hainfeld, L. Lin, D. N. Slatkin, F. Avraham Dilmanian, T. M. Vadas, and H. M. Smilowitz, Nanomed.: Nanotechnol., Biol. Med. **10**, 1609–1617 (2014).
[6] S. Lal, S. E. Clare, and N. J. Halas, Acc. Chem. Res. **41**, 1842–1851 (2008).
[7] G. v. Maltzahn, J.-H. Park, A. Agrawal, N. K. Bandaru, S. K. Das, M. J. Sailor, and S. N. Bhatia, Cancer Res. **69**, 3892–3900 (2009).
[8] D. P. O'Neal, L. R. Hirsch, N. J. Halas, J. D. Payne, and J. L. West, Cancer Lett. **209**, 171–176 (2004).
[9] N. Khlebtsov and L. Dykman, Chem. Soc. Rev. **40**, 1647–1671 (2011).
[10] I. Ojea-Jiménez, F. M. Romero, N. G. Bastús, and V. Puntes, J. Phys. Chem. C **114**, 1800–1804 (2010).
[11] K. Saha, S. S. Agasti, C. Kim, X. Li, and V. M. Rotello, Chem. Rev. **112**, 2739–2779 (2012).
[12] A. D. Phan, T. X. Hoang, T. H. L. Nghiem, and L. M. Woods, Appl. Phys. Lett. **103**, 163702 (2013).
[13] X. Ma, Y. Cheng, Y. Huang, Y. Tian, S. Wang, and Y. Chen, RSC Adv. **5**, 81682–81688 (2015).
[14] V. Biju, Chem. Soc. Rev. **43**, 744–764 (2014).
[15] N. Kawazoe and G. Chen, Biomaterials **54**, 226–236 (2015).
[16] X. Ji, R. Shao, A. M. Elliott, R. J. Stafford, E. Esparza-Coss, J. A. Bankson, G. Liang, Z.-P. Luo, K. Park, and J. T. Markert, J. Phys. Chem. C **111**, 6245–6251 (2007).
[17] L. Han, Y. Zhang, Y. Zhang, Y. Shu, X.-W. Chen, and J.-H. Wang, Talanta **171**, 32–38 (2017).
[18] R. Hu, M. Zheng, J. Wu, C. Li, D. Shen, D. Yang, L. Li, M. Ge, Z. Chang, and W. Dong, Nanomaterials **7**, 111 (2017).
[19] W. Feng, X. Zhou, W. Nie, L. Chen, K. Qiu, Y. Zhang, and C. He, ACS Appl. Mater. Interfaces **7**, 4354–4367 (2015).
[20] Y. Wang, F. Zhang, Q. Wang, P. Yang, H. Lin, and F. Qu, Nanoscale **10**, 14534–14545 (2018).
[21] E. Dulkeith, T. Niedereichholz, T. A. Klar, J. Feldmann, G. von Plessen, D. I. Gittins, K. S. Mayya, and F. Caruso, Phys. Rev. B **70**, 205424 (2004).
[22] J. Sun, J. P. Longtin, and T. F. Irvine, Jr., Int. J. Heat Mass Transfer **44**, 645–657 (2001).
[23] M. Yuan, Y. Wang, and Y. X. Qin, J. Biomed. Mater. Res., Part A **105**, 3350–3359 (2017).
[24] M. Yuan, Y. Wang, and Y.-X. Qin, Nanomed. Nanotechnol. Biol. Med. **14**, 1337–1347 (2018).
[25] U. Hohenester and A. Trügler, Comput. Phys. Commun. **183**, 370–381 (2012).